Title

Antigen-Specific CD4 T Cell and B Cell Responses to Borrelia burgdorferi.

Journal

The Journal of Immunology, 211(6)

ISSN

0022-1767

Authors

Hammond, Elizabeth M

Olsen, Kimberly J

Ram, Shivneel

et al.

Publication Date

2023-09-15

DOI

10.4049/jimmunol.2200890

Peer reviewed

Published in final edited form as:

J Immunol. 2023 September 15; 211(6): 994–1005. doi:10.4049/jimmunol.2200890.

Antigen-specific CD4 T cell and B cell responses to *Borrelia burgdorferi*

Elizabeth M. Hammond[1,2,3], **Kimberly J. Olsen**[2,3], **Shivneel Ram**[2,6], **Giang Vu Vi Tran**[2,3], **Laura S. Hall**[4], **John E. Bradley**[5], **Frances E. Lund**[5], **D. Scott Samuels**[4], **Nicole Baumgarth, DVM PhD**[1,2,3,7,8]

[1]Graduate Group in Immunology, University of California Davis;

[2]Center for Immunology and Infectious Diseases, University of California Davis;

[3]Department of Pathology, Microbiology, and Immunology, University of California Davis;

[4]Division of Biological Sciences, University of Montana;

[5]Department of Microbiology, University of Alabama, Birmingham;

[7]Department of Molecular Microbiology and Immunology and Department of Molecular and Comparative Pathobiology, Johns Hopkins University

Abstract

Long-lived T-dependent B cell responses fail to develop during persistent infection of mice with *Borrelia burgdorferi* (Bb), the causative agent of Lyme disease, raising questions about the induction and/or functionality of anti-Bb adaptive immune responses. Yet, a lack of reagents has limited investigations into Bb-specific T and B cells. We attempted two approaches to track Bb-induced CD4 T cells. First, a Bb mutant was generated with an influenza hemagglutinin peptide $HA_{111–119}$ inserted into the Bb Arp locus. While this Bb *arp*::HA strain remained infectious, peptide-specific T cell receptor transgenic CD4 T cells *in vitro*, or adoptively transferred into Bb *arp*::HA infected BALB/c mice did not clonally expand above that of recipients infected with the parental Bb strain or a Bb mutant containing an irrelevant peptide. Some expansion, however, occurred in Bb *arp*::HA-infected BALB/c SCID mice. Second, a newly identified I-A^b restricted CD4 T cell epitope $Arp_{(152–166)}$ was used to generate Arp MHCII tetramers. Flow cytometry showed small numbers of Arp-specific CD4 T cells emerging in mice infected with *Bb* but not with Arp-deficient *B. afzelii*. While up to 30% Arp-specific CD4 T cells were ICOS+ PD-1+ CXCR5+ BCL6+ Tfh, their numbers declined after day 12, before germinal centers (GCs) are prominent. Although some Arp-specific B cells, identified using fluorochrome-labeled recombinant Arp proteins, had the phenotype of GC B cells, their frequencies did not correlate with anti-Arp serum IgG. The data suggest a failure not in the induction, but maintenance of GC Tfh and/or B cells to Bb.

[8]**Correspondence:** Nicole Baumgarth, DVM PhD, W. Harry Feinstone Dept. Molecular Microbiology and Immunology, Bloomberg School of Public Health, Johns Hopkins University, 615 Wolfe Street, E4135, Baltimore, MD 21205, nbaumga3@jhmi.edu, (ph) 410 614 2718.

[6]Current address: San Francisco General Hospital, Clinical Lab, San Francisco, CA.

Introduction

Borrelia burgdorferi (Bb), a spirochete, causes Lyme disease in a variety of species, including humans (1), but causes persistent non-resolving infection with few if any disease manifestations in "reservoir species," such as small birds and rodents (2–5). Bb is transmitted to humans by the bite of adult blacklegged ticks of the genus *Ixodes*. Infection of ticks with Bb requires the presence of persistently infected reservoir hosts, as there is no vertical transmission of Bb from adult ticks to eggs (6). A number of Bb immune evasion mechanisms have been identified that support the establishment of chronic infection in these species. Among them are dynamic expression changes of immunogenic Bb surface antigens, which seems to allow the spirochete to evade antibody-mediated immunity and establish persistent infection (7). One example is the membrane lipoprotein outer surface protein (Osp) C. Although it is required for infection of a vertebrate host, once infection occurs OspC is rapidly downregulated, explaining the rather modest anti-OspC IgG titers observed in C57BL/6 mice following experimental infection (8, 9). Bb engineered to constitutively express OspC were rapidly eliminated from infected mice (10), demonstrating the importance of modulating OspC expression for immune evasion.

Bb also expresses the variable outer membrane lipoprotein VlsE which, using various expression cassettes, alters its antigenic surface profile, allowing Bb to evade antibody-mediated immunity (11, 12). Expression of VlsE on the surface of Bb has been proposed also to act as a "shield" that prevents recognition of other immunogenic surface antigens by the B cell response (13). Specifically, the absence of VlsE was reported to cause clearance of Bb in mice that were given antibodies to arthritis related protein (Arp) (13). Arp is a constitutively expressed outer membrane lipoprotein (14, 15). Although its function is unknown, its absence diminishes the infectivity of Bb spirochetes (16). Adoptive transfer of anti-Arp immune sera induced arthritis resolution in arthritis-susceptible strains of mice, but it did not induce bacterial clearance (17, 18). We previously showed that anti-Arp IgG responses are highly prevalent in C57BL/6 mice infected with Bb strain N40, and that the induction of anti-Arp IgG required the presence of CD40L and CD4 T cells (19, 20), thus cognate T dependent B cell activation. Despite the T-dependence of the anti-Arp IgG responses, antibiotic treatment rapidly reduced anti-Arp IgG serum titers to background levels, strongly suggesting a failure of the anti-Arp response to induce long-lived plasma cells (LLPC). In support of this hypothesis, we were unable to detect Arp-specific LLPC in the bone marrow and memory B cells (B_{mem}) in the spleen of Bb-infected mice for over 3 months (21). Furthermore, we demonstrated a rapid collapse of germinal centers (GCs) within four weeks after Bb infection (21). Given that GCs are the structures responsible for the induction of LLPC and B_{mem}, the anti-Arp response appears functionally defunct, but the mechanisms underlying this defect remain to be established.

Somewhat surprisingly, early studies suggested that the complete lack of T cells has little effect on the course of Bb infection (22, 23), while mice deficient in B cells were unable to control Bb infection and thus were shown to be indispensable for Bb-specific immunity (24). While this has led to the widely accepted model that control of Bb is B cell- but not T cell-mediated, the findings raise questions about the functionality of the induced CD4 T cells, as well as the nature of the B cell responses that seem to require no CD4 T cell help.

Because there are currently no tools available with which to assess Bb-specific CD4 T cell and T-dependent B cell responses in mice, and only one CD4 epitope of Bb had been defined previously in humans (25), we developed reagents with which to interrogate CD4 T and B cell responses in C57BL/6 mice. Using these tools we demonstrate a significant increase of Arp-specific CD4 Tfh and GC B cells but their rapid disappearance during Bb infection, suggesting that the lack of long-lived Arp-specific immunity is not due to a failure of their induction, but rather due to defective GC response maintenance.

Materials and Methods

B. burgdorferi strain construction

B31–5A4 was the background strain for the genetic constructs and *E. coli* TOP10F′ was used for cloning. The *arp*::HA and *arp*::Hm mutants were constructed as previously described (26, 27). The 3′ 841 nucleotides of the *arp* gene were amplified by PCR using KOD polymerase (Novagen) with oligonucleotides containing the $HA_{111–119}$ or mutated $HA_{111–119}$ (Hm) sequences, arp_996R+HA+AaAg or arp_996R+Hm+AaAg, respectively, and arp_155F (Table 1). The region downstream of *arp* was amplified with arp_978F+AatII and arp_D1773R+AgeI (Table 1). PCR products were cloned into pCR2.1-TOPO (Invitrogen) and confirmed by DNA-sequencing. The cloned PCR products were digested with AatII and AgeI and ligated together at the AatII site. The *flgBp-aacC1-trpLt* gentamicin resistant cassette containing flanking AatII sites was ligated between the fused *arp*::HA or *arp*::Hm DNA segment and the downstream DNA segment. The plasmids containing the *arp*::HA or *arp*::Hm and the *aacC1* selectable marker were purified and linearized using AhdI before electroporating competent B31–5A4 cells. Spirochetes were plated in liquid BSK in 96-well plates 24 h after transformation and transformants selected with 40 μg/ml gentamicin. Antibiotic-resistant cells were screened for the presence of the $HA_{111–119}$ or mutated $HA_{111–119}$ (Hm) sequences by PCR using the primers arp_780F and aacC1_R+AatII (Table 1), and the plasmid profiles of positive transformants were evaluated by multiplex PCR (28).

Mice and infections

BALB/c (000651), CBySmn.Cg-Prkdc^{scid}/J (BALB/c SCID, 001803), C57BL/6 (000664) and B6.Cg-*Prkdc*^{scid}/SzJ (B6-SCID, 001913) mice were purchased from The Jackson Laboratories, and housed under specific pathogen free conditions. TS-1 mice were a generous gift from Andrew Caton (Wistar Institute) (29), and were crossed with C.129S7(B6)-Rag1^{tm1Mom}/J (Jackson strain 003145, referred to as Rag1$^{-/-}$), in order to generate mice in which the only lymphocytes were HA-specific CD4 T cells (Rag1$^{-/-}$ × TS1). BALB/c mice were infected intranasally with 10 pfu Influenza A/Puerto Rico/8/34 (A/PR8), as described previously (30). For Bb infections, *arp*::HA, *arp*::Hm, strain B31–5A4, and strain N40 were grown in BSK II medium at 33°C under antibiotic selective conditions to log phase, and diluted in additional BSK II. BALB/c mice were injected intradermally in the intrascapular region with 5×10^5 spirochetes, and BALB/c scid mice were similarly injected with 2×10^5 spirochetes. To generate tissue-adapted spirochetes (19, 21), B6-SCID mice were injected intradermally with 1×10^5 low passage, cultured Bb N40. After at least 14 days of infection, ear tissue from B6-SCID mice was transplanted subcutaneously in the

right rear hock of 8–12 weeks old recipient female C57BL/6 mice leading to their infection. This mode of infection ensured that the right inguinal LN was always the infection-site draining LN. At various times after infection mice were euthanized by overexposure to CO_2 prior to harvesting tissues. All procedures were performed in strict accordance with protocols approved by the Animal Care and Use Committee of University of California, Davis.

Quantitative RT-PCR

Tissues from Bb infected mice were snap frozen on dry ice at the time of collection, then weighed. DNA extraction from tissues was performed using DNeasy Blood & Tissue Kit (Qiagen) according to manufacturer's protocols. RNA was extracted from cultured spirochetes using Aurum total RNA mini kit (BioRad), and cDNA was generated. Previously published primer and probe sequences (15) were used for amplification and detection of the *arp* and *flab* genes, respectively: arp-663F, arp-767R, and arp-705P; flab-571F, flab-677R, and flab-611P (Table 1). All assays included positive and negative controls. *Flab* copies per mg tissue were calculated based on a standard curve. Relative *arp* expression was calculated compared to *flab* expression.

Peptide libraries

Peptides representing 20-mer fragments overlapping by 5 amino acids covering residues 8 through 332 of the Arp sequence (NCBI reference WP_010890266.1) were generated by GenScript. 15-mer peptides overlapping by 5 amino acids were subsequently generated for regions of interest (approximately 40% of the Arp sequence). Individual lyophilized peptides were reconstituted according to manufacturer's instructions, using either water, or water mixed with ammonium hydroxide (NH_4OH), DMSO, or acetic acid (C_3HCOOH). PBS served as a no peptide control.

ELISPOT assay

96-well ELISPOT plates were coated with anti-IFNγ (clone AN-18, eBioscience) or anti-IL-2 (clone JES6–1A12, eBioscience) in PBS overnight, and blocked with 4% BSA as described previously (21). CD4 T cells from the draining LNs of 12-day Bb-infected mice were enriched by magnetic separation. Single cell suspensions of spleen cells from non-infected congenic mice were irradiated (3000 rad) and served as feeder cells. 1×10^5 CD4 T cells and 4×10^5 irradiated splenocytes were plated in each well, resuspended in RPMI culture media supplemented with 10% fetal calf serum. Varying concentrations of recombinant protein, peptide, or heat inactivated influenza A/Puerto Rico 8/34 virus were added for overnight culture at 37°C in 5% CO_2. Cytokine detection antibodies were added following lysis of the cells using water. Biotinylated anti-IFNγ (clone R4–6A2, eBioscience) or anti-IL-2 (clone JES6–5HA, eBioscience) and streptavidin conjugated to alkaline phosphatase (BD Pharmingen) was used to label secreted cytokines and spots were revealed using nitro-blue tetrazolium chloride (NBT)/5-bromo-4-chloro-3'-indolyphosphate p-toluidine salt (BCIP) substrate (Thermo Fisher). Spots were imaged and enumerated using an iSpot Spectrum EliSpot Reader System (Advanced Imaging Devices GmbH). Results were expressed as fold-change over control wells receiving PBS instead of protein or peptide.

ELISA assay

ELISA assay was performed as described previously (21). Briefly, 96-well ELISA plates (MaxiSorp, ThermoFisher) were incubated with 2 μg/ml rArp (GenScript) in PBS overnight (this and all subsequent incubations were performed at room temperature). After a 1 h block with 1% FBS and 0.1% milk powder in PBS/0.05% Tween 20, mouse sera were serially diluted in PBS and incubated for 2 h. Arp-specific antibody was revealed with biotinylated goat anti-mouse IgG (Southern Biotech), followed by a 1 h incubation with streptavidin-HRP (Vector Laboratories), then 20 min incubation with substrate (10 mg/ml 3,3′,5,5′-tetramethylbenzidine in 0.05 mM citric acid, 3% hydrogen peroxide). Reactions were stopped with 1 N sulfuric acid prior to measuring absorbance at 450 nm and 595 nm. Absorbance at 450 nm was subtracted from reference reading at 595 nm, then relative units of Arp-specific IgG were calculated based on a standard curve from sera pooled from Bb mice infected for 120 days.

Flow Cytometry

As described previously (21, 31), LNs and other tissues were dissociated between frosted glass slides and passed through a 70 μm nylon mesh filter to create single cell suspensions. If erythrocyte contamination was visible, then single cell suspensions were treated with ammonium chloride potassium (ACK) lysis buffer for 60 seconds and washed with staining media. Cell concentration was determined by hemacytometer count. Prior to antibody labeling, cells were treated with anti-CD16/CD32 (Fc block generated in-house; clone 2.4G2) and labeled with LIVE/DEAD Fixable Aqua Dead Cell Stain Kit (Invitrogen) for discrimination of live vs. dead cells. Cells were then stained with combinations of the following antibodies: CD3 (Alexa700 500A2 Invitrogen, PerCP-ef710 17A2 Invitrogen, FITC 2C11 in house), CD4 (Alexa700 RM4–5 Invitrogen, BUV395 RM4.5 BD Biosciences, APC GK1.5 Invitrogen, APC-ef780 GK1.5 Invitrogen), TS1 TCR (Biotin 6.5.2 in-house), CD19 (BV786 ID3 BD Biosciences, PE-CF594 ID3 Invitrogen,BUV737 ID3 BD Biosciences), CD45R (FITC RA3–6B2 in house, APC-ef780 RA3–6B2 Invitrogen), CD44 (BV711 IM7 Biolegend), CD11a (PE M17/4 Invitrogen, Cy7-PE M17/4 Invitrogen), ICOS (BUV395 C398.4A BD Biosciences), PD-1 (APC-ef780 J43 Invitrogen), CD8a (BUV737 53–6.7 BD Biosciences, AF700 53–6.7 Invitrogen), CD90.2 (Alexa700 30-H12 Biolegend), NK1.1 (Alexa700 PK136 Invitrogen), Gr-1 (red fluor 710 1A8 Tonbo), Ly6G (Alexa700 1A8-Ly6G BD Biosciences), F4/80 (Alexa700 BM8 Biolegend), CD11b (Alexa700 M1/70 Invitrogen), CXCR5 (BV785 L138D7 Biolegend), Bcl6 (PE-CF594 K112–91 BD Biosciences), TACI (BV421 8F10 BD Biosciences), CD24 (BV711 M1/69 BD Biosciences), CD138 (BV605 281–2 BD Biosciences), CD95 (BUV395 Jo2 BD Biosciences), CD38 (BUV737 90/CD38 BD Biosciences) and Streptavidin (APC Invitrogen).

Extracellular labeling was performed on ice for 20 min. For intracellular labeling, cells were fixed and permeabilized with Foxp3 Transcription Factor Staining Buffer Set (eBioscience) following manufacturer's instructions. Intracellular antibodies were incubated for 30 minutes at room temperature. Data was acquired on either a LSRFortessa or

FACSymphony flow cytometer (BD), and analyzed using FlowJo software. Population gates were determined with the help of fluorescence minus one (FMO) controls.

Protein kinase inhibitor (PKI) treatment

PKI treatment of single cell suspensions to enhance tetramer staining was performed as described previously (32). Briefly, a stock solution of Dasatinib (Selleck Chemical) was diluted to 1 mM in DMSO and stored at −20°C. LN single cell suspensions were incubated with a final concentration of 50 nM Dasatinib in 1X PBS at 37°C for 30 min. Cells were washed twice with staining media before proceeding to tetramer incubation and additional antibody labeling as outlined for flow cytometry.

Arthritis-related protein (Arp) “bait” generation

To identify Arp-specific B cells, we generated B-cell protein-tetramers (baits) using mono-biotinylated recombinant (r)Arp and fluorescently labeled streptavidin. The sequence Bb Arp 13–325 (GenBank accession number: AAL25643.1; https://www.ncbi.nlm.nih.gov/protein/16550916) followed by an AviTag was cloned into the pGEX−2T expression vector (Sigma-Aldrich) using restriction sites EcoRI and XhoI. The resulting expression construct produced rArp with an *N*−terminal GST tag and a C-terminal AviTag (GST−ARP−AviTag). Biotinylated rGST−Arp−AviTag was expressed in *E. coli* strain CVB101 (Avidity) and purified by FPLC using a GST HiTrap column (GE Healthcare) following the manufacturer’s recommended protocols. The GST tag was retained so the biotinylated rArp remained soluble. After exchange into PBS, biotinylated rGST−ARP−AviTag was titrated against fluorochrome-conjugated streptavidin (Prozyme). B cell baits were made by incremental addition of fluorochrome conjugated streptavidin to biotinylated GST−ARP−AviTag until the volumetric ratio for saturation was reached.

Tetramer labeling of CD4 T and B cells

I-E^d tetramers were loaded with $HA_{127–137}$ or $OmpF_{317–228}$ and conjugated to phycoerythrin (PE) by the NIH tetramer core. Single cell suspensions were incubated with tetramers at room temperature for 60 minutes, then washed with staining media before continuing to additional antibody staining on ice. I-A^b restricted $Arp_{152–166}$ MHC II tetramers conjugated to PE and Brilliant Violet 421 (BV421) fluorophores were also generated by the NIH Tetramer Core. Following PKI treatment of LN single cell suspensions, $Arp_{152–166}$ tetramers were incubated with cells for 60 min at room temperature, then washed with staining media before proceeding to Fc block and additional cell labeling. Similarly, tetrameric Arp B cell baits were incubated with single cell suspensions for 45 min at room temperature and washed with staining media prior to additional labeling as outlined under flow cytometry.

Results

A mutant Bb expressing an influenza hemagglutinin peptide fails to induce peptide specific CD4 T cells

We first aimed to use an existing CD4 T cell receptor (TCR) transgenic mouse to study antigen (Ag) specific responses to Bb infection. Such an approach has been used previously, including ovalbumin (OVA)-specific T cell responses in the context of infections with

Listeria monocytogenes (33, 34). In that study, *Listeria* was genetically engineered to express OVA, allowing measurement of OVA-specific, transgenic (OT-II) CD4 T cells instead of measuring responses to endogenous *Listeria* antigens both *in vitro* and *in vivo* (34). We aimed to use TS-1 TCR transgenic mice, which express an I-E^d restricted TCR specific for the influenza A epitope hemagglutinin ($HA_{111–119}$) (29). Given that Bb changes its gene expression profile as it adapts to various environments (35), we chose to insert the $HA_{111–119}$ peptide into a constitutively expressed Bb gene.

Insertion into the Bb flagellin (*flaB*, locus BB_RS00725), a constitutively expressed and essential gene for Bb structure and motility (36) resulted in non-infectious spirochetes with abnormal morphology (data not shown), likely due to disruption in the structure and function of the FlaB protein (37). We then inserted $HA_{111–119}$ into the arthritis related protein locus (encoded by *arp*, locus BB_RS05695), because it is constitutively expressed during Bb infection but plays a lesser role in Bb survival and infectivity. Rather, deletion of the *arp* gene only led to moderate reduction, not complete ablation, of infectivity (16). Thus, if the genetic manipulation results in reduced Arp function, then the mutant Bb should still be useful. The $HA_{111–119}$ nucleotide sequence as well as an E115K mutant $HA_{111–119}$ nucleotide sequence were integrated into the *arp* gene, generating the *arp*::HA strain and the *arp*::Hm negative control strain, respectively (Fig. 1A). The *arp*::HA and *arp*::Hm strains retained all plasmids essential for Bb infectivity, as tested by PCR (data not shown). Comparison of a*rp* expression in cultured *arp*::HA, *arp*::Hm, and the parental B31 strain, showed an approximate 2-fold decrease in *arp* expression in both mutants compared to the parental strain (data not shown).

Transfer of graded numbers CD4 T cells from Rag1 × TS-1 mice into BALB/c recipients infected with influenza A/PR8 showed a cell number-dependent increase in HA-specific CD4 T cell numbers recovered from the mice at day 10 after infection as measured using double labeling with an $HA_{111–119}$-tetramer and an idiotype-specific mAb for the TS-1 TCR (Supplemental Fig. 1A) (38). Therefore, the highest cell number tested (3.4×10^5) was transferred in subsequent experiments to measure HA-specific responses in recipient BALB/c and SCID mice infected with the *arp*::HA Bb, arp::Hm and the B31 parental strain via intradermal syringe injection (Fig. 1B). The *arp*::HA strain failed to induce a measurable HA-specific CD4 T cell response in BALB/c recipients greater than that observed infected with the two other strains (Fig. 1C–F and Supplemental Fig. 1B). Neither did we observe increased frequencies or total numbers TS-1 CD4 T cells in draining (d)LN (Fig. 1C) or spleen (Fig. 1D), nor increased frequencies of activated $CD11a^{hi}$ $CD44^{hi}$ T cells in these tissues (Fig. 1E, F and Supplemental Fig. 1B). When we used T and B cell-deficient BALB/c SCID mice as TS-1 recipients, we noted a somewhat greater responses to *arp*::HA mutant infections compared to the controls, with increases in TS-1 T cell frequencies and total numbers that reached statistical significance in the spleen (Fig. 1G, H) as well as significant increases in activated $CD11a^{hi}$ $CD44^{hi}$ TS-1 CD4 T cells (Fig. 1I, J and Supplemental Fig. 1C). The increases in TS-1 activation in BALB/c SCID mice compared to immunocompetent BALB/c mice might be due to decreased bacterial clearance in the SCID recipients, and thus greater availability of the HA antigen (Supplemental Fig. 1D, E). There was no significant difference in bacterial burden between groups infected with the *arp*::HA, *arp*::Hm, and B31 parental strains, indicating that the insertion of the $HA_{111–119}$ and E115K

epitopes into the *arp* locus did not appear to significantly impact infectivity (Supplemental Fig. 1D, E).

As the failure of arp::HA to induce a robust response from HA-specific TS-1 cells seemed to be due to limited antigen availability *in vivo*, we assessed the ability of the *arp*::HA strain to induce TS-1 responses *in vitro* by stimulating magnetically enriched CFSE-labeled CD4 T cells specific for $HA_{111–119}$ ($Rag1^{-/-}$ × TS1), or non-specific polyclonal control CD4 T cells (BALB/c) for 72 h with *arp*::HA spirochetes or *arp*::Hm controls (Fig. 1K, L). TS-1 CD4 T cell proliferation was low after stimulation with the HA mutant and comparable to that of T cells left unstimulated or stimulated with the Hm mutant as assessed by CFSE dilution. In contrast, and as expected, HA-specific CD4 T cells were highly proliferative after stimulation with influenza A/PR/8 (Fig. 1K). There was also no proliferation observed following stimulation of polyclonal CD4 T cells from BALB/c mice (Fig 1L). Thus, despite successful insertion of the HA-peptide, the *arp*::HA Bb strain did not consistently stimulate HA-specific CD4 T cells *in vivo* or *in vitro*.

Identification of an I-A^b restricted epitope of Arp using IL-2 ELISPOT

Measurement of antigen-specific CD4 T cell responses in the context of a polyclonal T cell response has been facilitated through the generation of MHCII-peptide complexes that, when oligomerized, can label CD4 T cells for analysis by flow cytometry. Given the inability of the mutant Bb to induce transgenic T cell activation, we aimed next to develop an MHCII-restricted tetramer to study Bb-specific CD4 T cell responses in wild type C57BL/6 mice. We evaluated the constitutively expressed Arp protein of Bb N40 as a candidate target because we and others had shown previously that it is immunogenic and induces strong, T-dependent IgG responses after infection of C57BL/6 mice with Bb strain N40 (17, 39). Furthermore, the use of Arp may also allow studies of T cell responses to other Bb strains, as comparison of the *arp* gene from Bb strain N40 (accession NC_017415.1, https://www.ncbi.nlm.nih.gov/nuccore/NC_017415.1, locus tag BBUN40_RS05425) using BLAST demonstrated that at least eight strains of *B. burgdorferi*, including the commonly used laboratory strain B31, carried the *arp* gene (Table 2). Comparison of the Bb Arp protein sequences revealed a high degree of homology across all Arp sequences (>90%). Notably, strain B31 was among the five Bb strains that shared an identical Arp sequence with N40. In contrast, the closely related Lyme disease spirochetes *Borrelia afzelii* (accession GCF_000222835.1, https://www.ncbi.nlm.nih.gov/assembly/GCF_000222835.1/) and *Borrelia garinii* (accession GCF_003814405.1, https://www.ncbi.nlm.nih.gov/assembly/GCF_003814405.1/) lack *arp* (Table 2).

CD4 T cells from dLN of mice infected with Bb strain N40 were more responsive to *in vitro* stimulation with rArp protein than CD4 T cells from uninfected controls, suggesting that Arp-specific CD4 T cells are induced after Bb infection (Fig. 2A). Therefore, we isolated CD4 T cells from these LNs to screen 20-mer peptides, overlapping by 5 amino acids, and spanning residues 8 through 332 of Arp (NCBI accession WP_010890266.1, https://www.ncbi.nlm.nih.gov/protein/WP_010890266.1/), for their ability to induce cytokine secretion. Since the CD4 T cell response to Bb is considered Th1 dominant (40–42), we first measured IFNγ production by ELISPOT. We included mediastinal LN CD4 T cells

from day 7 influenza A/PR8-infected mice, restimulated with heat-inactivated A/PR8, as a positive control. While the influenza controls showed strong increases in IFNγ ELISPOTs when compared to the negative control wells without peptides, stimulation of CD4 T cells from Bb-infected mice with recombinant Arp or Arp peptides resulted in at best very modest induction of IFNγ ELISPOTS (Fig. 2B). Similar results were obtained also when we isolated CD4 T cells from mice infected with Bb via syringe inoculation, as well as mice infected with tissue adapted spirochetes for one year (data not shown). Thus, the failure to measure IFNγ ELISPOTs after Arp stimulation was not due to technical difficulties with the IFNγ ELISPOT, the mode of infection, or the time point at which we harvested the T cells. Furthermore, given the proliferative response of CD4 T cells at 21 dpi (Fig. 2A) and the presence of activated CD4 T cells in the dLN of Bb-infected mice at 12 dpi (20, 21), our data suggested that Bb infection did not induce IFNγ -producing LN CD4 T cells.

Since IL-2 is secreted by CD4 T cells following TCR engagement (43), we assessed IL-2 ELISPOT generation in these cultures and found significant IL-2 secretion (Fig. 2C) The drawback in using IL-2 as a readout for TCR engagement is the potential for higher background in ELISPOT assays, as naïve T cells can secrete IL-2 (44). To overcome this limitation, we calculated the fold-change of spots obtained from peptide stimulated wells compared to the mean number of spots seen in the PBS control wells. Using this approach, we found that stimulation of LN CD4 T cells with rArp consistently resulted in robust IL-2 ELISPOT-induction compared to the control wells (Fig. 2C). Screening the Arp peptide library at least three times consistently resulted in strong increases in IL-2 ELISPOTs above background in cultures containing peptide fragments F22 and F23, and less strong induction in ELISPOTs from additional Arp regions (Fig. 2C).

We then conducted a similar screen using shorter 15-mer Arp peptides offset by 5 amino acids, spanning regions of interest from our initial screen. The highest number of IL-2 ELISPOTs was induced by a 15-mer peptide “B11”, which shared overlapping amino acid sequences with peptides F22 and F23 (Fig. 2D). No other peptide induced significant and reproducible IL-2 ELISPOTs (Fig. 2D), suggesting the presence of at least one T cell epitope in this region of Arp. To more precisely determine the epitope sequence included in peptide B11, we screened the original B11 15-mer peptide as well as additional peptides generated by exchanging 1, 2 or 3 amino acid residues upstream (−1, −2 and −3), or downstream (+1, +2 and +3) of the original B11 sequence. T cell stimulation via B11 (+3), spanning Arp residues 152 to 166, resulted in the largest number of IL-2 ELISPOTs. The spot counts were comparable to those observed with the full length rArp, suggesting that we identified a major I-A^b-restricted epitope on Arp (Fig. 2E, F). As little as 5 ng of $Arp_{152–166}$ induced significant increases in IL-2 ELISPOTs compared to PBS (Fig. 2G), indicating the high immunogenicity of this peptide. Consistent with induction of ELISPOTs by peptides F22 and F23, the $Arp_{152–166}$ sequence spanned these originally identified immunogenic regions (Fig. 2H).

Validation of the I-A^b restricted Arp Tetramer $Arp_{152–166}$

Due to the low affinity of TCR interactions with soluble peptide-MHC class II (pMHCII) molecules, tetrameric pMHCII molecules have been developed to identify CD4 T cells

expressing antigen-specific TCRs (45). MHC class II tetramers have proved invaluable in following CD4 T cell responses in non-TCR transgenic models of infection and immunization (46). Using the above identified $Arp_{152–166}$ (TIDFYIEPRPISSFL) peptide, the NIH Tetramer Core Facility generated two MHCII ($I\text{-}A^b$) peptide tetramer complexes, one labeled with phycoerythrin (PE) and the other with Brilliant Violet 421 (BV421). Cell populations stained with only one tetramer likely constitute non-specific binding to non-peptide components of the tetramer. However, using dual staining with these tetramers, approximately 0.05 – 0.2% of CD4 T cells in the draining inguinal LNs of Bb infected mice stained with both tetramers at 14 dpi (Fig. 3A, B). To determine whether we could further optimize the identification of Arp-specific CD4 T cells, we treated cells with Dasatinib, a protein kinase inhibitor (PKI) prior to tetramer incubation. PKI treatment increases the number of TCR molecules retained on the cell surface, potentially increasing tetramer binding and staining intensity (32), in other words, enhancing the mean fluorescence intensity (MFI) of the tetramer-bound cells (32, 47). As expected, PKI treatment did not affect the number of cells that bound the Arp tetramer (Fig. 3B). It did, however, result in modest increases in the MFI of the PE-labeled but not the BV421-labeled tetramer (Fig. 3C). We therefore treated all subsequent samples with PKI prior to tetramer labeling.

We conducted several studies to confirm that the Arp tetramer identified Bb-induced antigen-specific CD4 T cells. First, we tested whether Bb infection increased the number of Arp-tetramer binding cells. For that we performed a magnetic pull-down assay first using PE-labeled Arp-tetramers to stain LN CD4 T cells from Bb-infected and non-infected controls and then using anti-PE antibodies conjugated to magnetic beads (Fig. 3D). The pull down resulted in an at least fifty-fold increase in the frequency of Arp-specific CD4 T cells among total LN cells from 14 dpi with Bb, compared to frequencies measured prior to enrichment (2.55% ± 0.41% and 0.0492% ± 0.0066%, respectively; Fig. 3E). In contrast, use of LN cells from naïve mice, resulted in only a modest enrichment in the number of Arp-specific CD4 T cells (Fig. 3E). Presumably these cells constituted the Arp-specific CD4 T cells of the naïve repertoire. Their frequencies (0.0129% ± 0.0113% of total tetramer-enriched lymphocytes, Fig. 3E) are similar to precursor frequencies reported for other systems (48–50).

To ensure that infection did not lead to an increase in non-specific expansion of tetramer-binding cells, we quantified Arp tetramer-stained CD4 T cells also in mice infected with the *B. afzelii* strain PKo, a closely related Lyme disease spirochete that lacks the *arp* gene (Table 2). *B. afzelii* infection induced a CD4 response of similar magnitude to that induced by Bb in the draining LN at 14 dpi (3.3-fold increase in total number of CD4 and 3.8-fold increase, respectively, compared to naïve LN). Yet, the total number of Arp tetramer binding CD4 T cells detectable in these mice was not significantly different from that of non-infected controls, and they also did not differ from the number of CD4 T cells that bound to two control tetramers of irrelevant specificity in Bb-infected LN (Fig. 3F). These data showed that $Arp_{152–166}$ tetramer-bound CD4 T cells recognize a Bb-specific antigen and expand in response to infection with Arp-expressing but not Arp non-expressing spirochetes. A Bb-specific expansion of $Arp_{152–166}$ -specific CD4 T cells was further supported by data showing that >80% of Arp-tetramer positive CD4 T cells were enriched for T cells expressing an activated ($CD44^{hi}$ $CD11a^{hi}$) phenotype (Fig. 3G).

Together, the data demonstrated that the I-A^b tetramer displaying Bb $Arp_{152–166}$ reliably identified Bb-specific CD4 T cells generated during infection with Arp-expressing but not Arp-deficient *Borrelia* spirochetes. The increased numbers of Arp-specific CD4 T cells detectable 14 dpi compared to either uninfected mice, or mice infected with a *Borrelia* strain lacking Arp, demonstrates furthermore that the tetramer-binding Arp-specific CD4 T cells are induced and undergo clonal expansion *in vivo* in a Bb-specific manner.

Tetramer-positive CD4 T cells display modest expansion and a robust Tfh phenotype

The kinetics (Fig. 4A) and phenotype (Fig. 4B) of total and Arp-specific CD4 T cells to Bb N40 infection was assessed in dLN of individual mice by flow cytometry. The highest numbers of tetramer-binding CD4 T cells were found between 8–12 dpi, with an average of $8.5 \times 10^3 \pm 3.6 \times 10^3$ Arp-specific CD4 T cells per dLN (mean ± SD for 8, 9, and 12 dpi combined, n=4 mice each timepoint). By 14 dpi that number had dropped to $1.9 \times 10^3 \pm 6.7 \times 10^2$ (mean ± SD, n=4 mice) Fig. 4A). Even at the height of the Arp-specific CD4 T cell response, increases in total numbers of Arp-specific CD4 T cells were modest, consistent with our previous observations of a modest increase in dLN CD4 T cells, but in contrast to the development of a robust T-dependent anti-Arp IgG responses (8, 17, 19). Furthermore, the peak in Arp-specific CD4 T cell numbers seemed to precede that of GCs following Bb infection (Fig. 5 (8, 21)). Nonetheless, many of the Arp-specific CD4 T cells displayed classical markers of Tfh including ICOS, PD-1, and CXCR5, and roughly 30% also expressed the transcription factor of Tfh polarization, Bcl6 (Fig. 4B; (51–53)) and, consistent with the robust Arp-specific IgG response seen in Bb infection, they were more strongly enriched for Tfh compared to the other dLN CD4 T cells (Fig. 4C). Thus, although induced, a strong contraction of Arp-Tfh occurred around the time of, or even preceding the time of GC onset, around 12–15 dpi ((8, 21) and Fig. 5).

Early decline of Arp-specific GC B cells

We next quantified Arp-specific plasmablasts, plasma cells and GC B cells by generating tetrameric recombinant Arp “baits” labeled with PE or allophycocyanin (APC), labeling dLN of C57BL/6 mice infected with host-adapted spirochetes at various times after infection. We gated on live, CD19+, Arp-bait double-positive cells to identify Arp-specific B cells (Fig. 5A and Supplemental Fig. 2A). Similar to the kinetics of Arp-specific CD4 T cells, Arp-specific CD19+ B cells were most numerous in the dLN early in the response to Bb infection (at 7 and 9 dpi) and dropped sharply in number by 12 dpi (Fig. 5A). Among those cells, extrafollicular foci (EF) plasmablasts (PB)/ plasma cells (PC) were identified as $CD19^{lo}$ $CD45R^{lo}$ $TACI^{hi}$ CD138+ (Supplemental Fig. 2B). Total EF responses peaked around 12 dpi, while the Arp-specific EF PC/PB numbers were quite variable, following a modest peak at 7 dpi (Fig. 5B). While the $CD19^{lo}$ $CD45R^{lo}$ Arp-specific B cells strongly upregulated the cytokine receptor TACI, a sign of their differentiation towards a plasmablast fate, many of these cells failed to upregulate CD138 (Supplemental Fig. 2B). Among $CD45R^{hi}$ CD19+ B cells, the frequencies of Arp-specific B cells with classical GC B cell phenotype (CD95+ $CD24^{hi}$) emerged around day 12 – 14 dpi (Supplemental Fig. 2C, D), while total numbers increased earlier (Fig. 5C). Among the $CD45R^{hi}$ CD95+ Arp+ B cells at least 50% showed the additional GC phenotype $CD38^{lo}$ already by day 7 (Supplemental Fig. 2E, F), when GC are histologically not yet present (20, 54) (Supplemental Fig. 2C, D),

suggesting that CD24 upregulation may provide a more useful marker for GC B cells during Bb infection and was thus used for quantification of total and Arp-specific GC B cells (Fig. 5C).

As expected, Bb-infected mice had robust serum Arp-IgG levels (Fig. 5D). These levels did not correlate with the number of Arp+ GC B cells at 18 dpi, several days after formation of GCs ((21); p=0.64 Pearson's correlation, Fig. 5E). Together these data further demonstrate the lack of robust Arp-specific GC B cell responses. While Arp-specific CD4 Tfh and B cells were induced after Bb infection, they did not seem to be maintained.

Discussion

In response to infections, B cells are known to form extrafollicular responses that result in the rapid differentiation of B cells to plasma cells, generating antibodies that have undergone little affinity maturation, as well as germinal centers (reviewed in (55)). Our previous work demonstrated the formation of germinal centers (GCs) in lymph nodes around 15 days after Bb infection in C57BL/6 mice and their rapid collapse around 2 weeks later (8, 21) for reasons that remain to be established. Despite the presence of these GCs for about 2 weeks, we were unable to detect either bone marrow LLPC or B_{mem}, and at best transient affinity maturation to Arp (8, 20, 21). Thus, the data suggested that GC responses to Arp were either never induced, or that they were not functional. Here we developed tools with which we demonstrate the induction of both, GC B cells and GC CD4 Tfh with antigen receptor specificity to Arp. This data is significant, as it provides further evidence that CD4 T cell and B cell responses to Bb are initiated but do not result in the establishment of long-lived, affinity-matured humoral immunity. The observed lack of correlation between the frequencies of GC Arp-specific B cells and levels of serum anti-Arp IgG further suggests that the antibody response to Bb is not derived from GC responses. A mainly plasmablast derived response would also explain the ongoing production of both IgM and IgG for months after Bb infection ((56) and Hastey, CJ et al, submitted). Of note, the spleen does not contain significant numbers of Bb-specific antibody secreting cells at any time after Bb infection, as we showed previously (19). Yet, even among the plasmablasts we noted a lack of CD138 upregulation, a surface receptor important for long-term plasmablast/cell survival (57), further explaining the failure of maintain Bb-specific antibody levels following antibiotic treatment (8).

It remains puzzling why the GCs are unable to induce B_{mem} and LLPC. While LLPC were reported to emerge only late in the GC response (58) and thus the short-lived nature of the GCs could have potentially impeded their development, B_{mem} have been shown to rapidly emerge from GC responses in various model systems, and may also be generated through extrafollicular responses (55), thus suggesting other explanations are likely responsible. We had shown previously that the lymph node architecture is severely affected by Bb infection of C57BL/6 mice, destroying the demarcation of T and B cell zones (8, 19, 54), and that FDCs seem to lack deposition of complement C4 (8). Whether these alterations are at the heart of the defective GC response remains to be established. The data provided here clearly demonstrate that Arp-specific T and B cells are induced, however, that neither a robust clonal expansion nor maintenance of these cells is seen. It is our hypothesis that this failure

of GC response maintenance provides a mechanism that allows for Bb persistence. The developed tools will be critical in identifying potential CD4 Tfh- and/or B cell-intrinsic functional defects in the future, as these cells can now be identified, isolated, and studied.

To study Bb-specific CD4 T cell responses we focused on Arp, a constitutively expressed and highly conserved Bb protein for which we identified a MHCII I-A^b restricted epitope. Utilizing this epitope in two differently fluorochrome-labeled MHCII-tetramers identified 0.05–0.2% of activated polyclonal LN CD4 T cells as Arp specific at the height of the LN response. Many of these CD4 T cells had a phenotype consistent with that of GC Tfh, as we would have expected, given the robust anti-Arp IgG response in Bb-infected mice. Likewise, using the recombinant Arp as a bait, we were able to demonstrate a comparable small fraction of Arp-specific GC B cells. Thus, these tools now allow for the first-time studies on CD4 and B cells specific to the same Bb antigen in the polyclonal response to Bb infection in wild type mice.

An acknowledged limitation of the generated MHCII tetramers and antigen-baits is the small frequency of Arp-specific CD4 T and B cells that we were able to identify. Given the strong T-dependent B cell responses to Arp we and others had identified in these Bb-infected mice (17, 19, 20), we had expected a more robust proportion of the adaptive response to be directed against Arp. However, the sheer number of Bb-expressed proteins, considered to be in the hundreds, might explain this finding (59). We had initially tried to circumvent this challenge by inserting a small peptide of influenza A/PR/8 into Bb strain B31, with which we hoped to then see the stimulation of CD4 TCR transgenic T cells specific for this peptide after Bb infection. Use of such a TCR transgenic would have allowed us to increase the number of antigen-specific naïve T cells prior to infection via adoptive transfer, as successfully done with other models (33, 34). Unfortunately, even when we succeeded in overcoming the well-known challenge of genetically manipulating Bb without losing infectivity (60), we were nonetheless unsuccessful in generating a mutant that generated immunogenic HA-peptides able to stimulate the TCR transgenic CD4 T cells either *in vivo* in immunocompetent mice or *in vitro*, although *arp* was expressed and responses could be seen in SCID mice. There are several possibilities why the *arp*::HA strain was unable to induce an HA-specific T cell response in BALB/c mice. Bb expresses a large number of potentially antigenic lipoproteins (61, 62), inducing a complex, polyclonal immune response (19, 63). It is possible that the $HA_{111–119}$ epitope is less immunogenic than endogenous Bb antigens in the context of this complex pathogen. Alternatively, processing and loading of the $HA_{111–119}$ peptide sequence into MHC II molecules may have been affected by its incorporation into the Arp protein. The findings of TS-1 T cell activation in SCID mice, which have at least 10-fold higher Bb burden than immunocompetent BALB/c mice may suggest a lack of sufficient antigen availability. While this attempt proved unsuccessful, it is noteworthy that the *arp* locus was amenable to the genetic manipulation and might be a useful target for future attempts to express antigens by Bb. In contrast, insertion of the HA-peptide into the *flab* locus, yielded Bb with abnormal morphology that were unable to establish infection in C57BL/6 mice.

The reagents generated allowed us to determine that the failure to generate Arp-specific LLPC and B_{mem} after Bb infection, and the resulting rapid disappearance of protection from

re-infection and Arp-specific serum IgG after antibiotic treatment (8) is not due to a failure to induce Arp-specific GC Tfh and B cells, but an inability to maintain these responses.

Supplementary Material

Refer to Web version on PubMed Central for supplementary material.

Acknowledgements

The authors would like to thank Tracy Rourke (UC Davis) for expert support with flow cytometry, the NIH Tetramer Core Facility (contract number 75N93020D00005) for providing the Arp MHC II tetramers utilized herein, and Dr. Shilpa Sachan (Johns Hopkins University) for advice with data analysis and discussions.

This work was supported by grants from the Global Lyme Alliance (N.B.), the Stephen and Alexandra Cohen Foundation (N.B.), NIH T32 AI060555 (E.M.H), NIH/NIAID R01AI157007 (N.B.), R01AI051486 (D.S.S) and U19AI142737 (F.E.L).

Abbreviations:

Arp	arthritis related protein
Bb	Borrelia burgdorferi
B_{mem}	memory B cells
dpi	days post infection
EF	extrafollicular foc
GC	germinal center
HA	hemagglutinin
LN	lymph node
LLPC	long-lived plasma cells
TCR	T cell receptor

References

1. Steere AC, Strle F, Wormser GP, Hu LT, Branda JA, Hovius JW, Li X, and Mead PS. 2016. Lyme borreliosis. Nature reviews. Disease primers 2: 16090.
2. Bunikis J, Tsao J, Luke CJ, Luna MG, Fish D, and Barbour AG. 2004. Borrelia burgdorferi Infection in a Natural Population of Peromyscus Leucopus Mice: A Longitudinal Study in an Area Where Lyme Borreliosis Is Highly Endemic. The Journal of Infectious Diseases 189: 1515–1523. [PubMed: 15073690]
3. Tilly K, Rosa PA, and Stewart PE. 2008. Biology of Infection with Borrelia burgdorferi. Infectious Disease Clinics of North America 22: 217–234. [PubMed: 18452798]
4. Radolf JD, Caimano MJ, Stevenson B, and Hu LT. 2012. Of ticks, mice and men: understanding the dual-host lifestyle of Lyme disease spirochaetes. Nat Rev Microbiol 10: 87–99. [PubMed: 22230951]
5. Helble JD, McCarthy JE, and Hu LT. 2021. Interactions between Borrelia burgdorferi and its hosts across the enzootic cycle. Parasite Immunol 43: e12816. [PubMed: 33368329]

6. Rollend L, Fish D, and Childs JE. 2013. Transovarial transmission of Borrelia spirochetes by Ixodes scapularis: A summary of the literature and recent observations. Ticks and Tick-borne Diseases 4: 46–51. [PubMed: 23238242]
7. Tracy KE, and Baumgarth N. 2017. Borrelia burgdorferi Manipulates Innate and Adaptive Immunity to Establish Persistence in Rodent Reservoir Hosts. Front Immunol 8: 116. [PubMed: 28265270]
8. Elsner RA, Hastey CJ, Olsen KJ, and Baumgarth N. 2015. Suppression of long-lived humoral immunity following Borrelia burgdorferi induced Lyme disease. PLoS Pathog 11: e1004976. [PubMed: 26136236]
9. Tilly K, Krum Jonathan G, Bestor A, Jewett Mollie W, Grimm D, Bueschel D, Byram R, Dorward D, VanRaden Mark J, Stewart P, and Rosa P. 2006. Borrelia burgdorferi OspC Protein Required Exclusively in a Crucial Early Stage of Mammalian Infection. Infection and Immunity 74: 3554–3564. [PubMed: 16714588]
10. Xu Q, Seemanapalli SV, McShan K, and Liang FT. 2006. Constitutive Expression of Outer Surface Protein C Diminishes the Ability of Borrelia burgdorferi To Evade Specific Humoral Immunity. Infection and Immunity 74: 5177–5184. [PubMed: 16926410]
11. Zhang J-R, Hardham JM, Barbour AG, and Norris SJ. 1997. Antigenic Variation in Lyme Disease Borreliae by Promiscuous Recombination of VMP-like Sequence Cassettes. Cell 89: 275–285. [PubMed: 9108482]
12. Bankhead T, and Chaconas G. 2007. The role of VlsE antigenic variation in the Lyme disease spirochete: persistence through a mechanism that differs from other pathogens. Molecular Microbiology 65: 1547–1558. [PubMed: 17714442]
13. Lone AG, and Bankhead T. 2020. The Borrelia burgdorferi VlsE Lipoprotein Prevents Antibody Binding to an Arthritis-Related Surface Antigen. Cell Reports 30: 3663–3670.e3665. [PubMed: 32187539]
14. Hodzic E, Feng S, Freet KJ, Borjesson DL, and Barthold SW. 2002. Borrelia burgdorferi population kinetics and selected gene expression at the host-vector interface. Infect Immun 70: 3382–3388. [PubMed: 12065476]
15. Hodzic E, Feng S, Freet KJ, and Barthold SW. 2003. Borrelia burgdorferi population dynamics and prototype gene expression during infection of immunocompetent and immunodeficient mice. Infect Immun 71: 5042–5055. [PubMed: 12933847]
16. Imai D, Holden K, Velazquez EM, Feng S, Hodzic E, and Barthold SW. 2013. Influence of arthritis-related protein (BBF01) on infectivity of Borrelia burgdorferi B31. BMC microbiology 13: 100. [PubMed: 23651628]
17. Feng S, Hodzic E, and Barthold SW. 2000. Lyme arthritis resolution with antiserum to a 37-kilodalton Borrelia burgdorferi protein. Infect Immun 68: 4169–4173. [PubMed: 10858233]
18. Feng S, Hodzic E, Freet K, and Barthold SW. 2003. Immunogenicity of Borrelia burgdorferi arthritis-related protein. Infect Immun 71: 7211–7214. [PubMed: 14638819]
19. Tunev SS, Hastey CJ, Hodzic E, Feng S, Barthold SW, and Baumgarth N. 2011. Lymphoadenopathy during lyme borreliosis is caused by spirochete migration-induced specific B cell activation. PLoS Pathog 7: e1002066. [PubMed: 21637808]
20. Elsner RA, Hastey CJ, and Baumgarth N. 2015. CD4+ T cells promote antibody production but not sustained affinity maturation during Borrelia burgdorferi infection. Infect Immun 83: 48–56. [PubMed: 25312948]
21. Hastey CJ, Elsner RA, Barthold SW, and Baumgarth N. 2012. Delays and diversions mark the development of B cell responses to Borrelia burgdorferi infection. Journal of immunology (Baltimore, Md. : 1950) 188: 5612–5622. [PubMed: 22547698]
22. Fikrig E, Barthold SW, Chen M, Chang CH, and Flavell RA. 1997. Protective antibodies develop, and murine Lyme arthritis regresses, in the absence of MHC class II and CD4+ T cells. The Journal of Immunology 159: 5682–5686. [PubMed: 9548512]
23. McKisic MD, and Barthold SW. 2000. T-cell-independent responses to Borrelia burgdorferi are critical for protective immunity and resolution of lyme disease. Infect Immun 68: 5190–5197. [PubMed: 10948143]

24. Belperron AA, Dailey CM, Booth CJ, and Bockenstedt LK. 2007. Marginal Zone B-Cell Depletion Impairs Murine Host Defense against Borrelia burgdorferi Infection. Infection and Immunity 75: 3354–3360. [PubMed: 17470546]
25. Meyer AL, Trollmo C, Crawford F, Marrack P, Steere AC, Huber BT, Kappler J, and Hafler DA. 2000. Direct enumeration of Borrelia-reactive CD4 T cells ex vivo by using MHC class II tetramers. Proceedings of the National Academy of Sciences 97: 11433–11438.
26. Drecktrah D, Hall LS, Crouse B, Schwarz B, Richards C, Bohrnsen E, Wulf M, Long B, Bailey J, Gherardini F, Bosio CM, Lybecker MC, and Samuels DS. 2022. The glycerol-3-phosphate dehydrogenases GpsA and GlpD constitute the oxidoreductive metabolic linchpin for Lyme disease spirochete host infectivity and persistence in the tick. PLOS Pathogens 18: e1010385. [PubMed: 35255112]
27. Samuels DS, Drecktrah D, and Hall LS. 2018. Genetic Transformation and Complementation. In Borrelia burgdorferi: Methods and Protocols. Pal U, and Buyuktanir O, eds. Springer New York, New York, NY. 183–200.
28. Bunikis I, Kutschan-Bunikis S, Bonde M, and Bergström S. 2011. Multiplex PCR as a tool for validating plasmid content of Borrelia burgdorferi. Journal of Microbiological Methods 86: 243–247. [PubMed: 21605603]
29. Kirberg J, Baron A, Jakob S, Rolink A, Karjalainen K, and von Boehmer H. 1994. Thymic selection of CD8+ single positive cells with a class II major histocompatibility complex-restricted receptor. The Journal of Experimental Medicine 180: 25–34. [PubMed: 8006585]
30. Nguyen TTT, Graf BA, Randall TD, and Baumgarth N. 2017. sIgM–FcμR Interactions Regulate Early B Cell Activation and Plasma Cell Development after Influenza Virus Infection. The Journal of Immunology 199: 1635–1646. [PubMed: 28747342]
31. Rothaeusler K, and Baumgarth N. 2006. Evaluation of intranuclear BrdU detection procedures for use in multicolor flow cytometry. Cytometry. Part A : the journal of the International Society for Analytical Cytology 69: 249–259. [PubMed: 16538653]
32. Lissina A, Ladell K, Skowera A, Clement M, Edwards E, Seggewiss R, van den Berg HA, Gostick E, Gallagher K, Jones E, Melenhorst JJ, Godkin AJ, Peakman M, Price DA, Sewell AK, and Wooldridge L. 2009. Protein kinase inhibitors substantially improve the physical detection of T-cells with peptide-MHC tetramers. Journal of Immunological Methods 340: 11–24. [PubMed: 18929568]
33. Pope C, Kim S-K, Marzo A, Williams K, Jiang J, Shen H, and Lefrançois L. 2001. Organ-Specific Regulation of the CD8 T Cell Response to *Listeria monocytogenes* Infection. The Journal of Immunology 166: 3402–3409. [PubMed: 11207297]
34. Foulds KE, Zenewicz LA, Shedlock DJ, Jiang J, Troy AE, and Shen H. 2002. Cutting edge: CD4 and CD8 T cells are intrinsically different in their proliferative responses. Journal of immunology (Baltimore, Md. : 1950) 168: 1528–1532. [PubMed: 11823476]
35. Samuels DS, Lybecker MC, Yang XF, Ouyang Z, Bourret TJ, Boyle WK, Stevenson B, Drecktrah D, and Caimano MJ. 2021. Gene Regulation and Transcriptomics. Curr Issues Mol Biol 42: 223–266. [PubMed: 33300497]
36. Motaleb MA, Corum L, Bono JL, Elias AF, Rosa P, Samuels DS, and Charon NW. 2000. Borrelia burgdorferi periplasmic flagella have both skeletal and motility functions. Proceedings of the National Academy of Sciences of the United States of America 97: 10899–10904. [PubMed: 10995478]
37. Sultan SZ, Manne A, Stewart PE, Bestor A, Rosa PA, Charon NW, and Motaleb MA. 2013. Motility is crucial for the infectious life cycle of Borrelia burgdorferi. Infect Immun 81: 2012–2021. [PubMed: 23529620]
38. Hataye J, Moon JJ, Khoruts A, Reilly C, and Jenkins MK. 2006. Naïve and Memory CD4+ T Cell Survival Controlled by Clonal Abundance. Science 312: 114–116. [PubMed: 16513943]
39. Sette A, Moutaftsi M, Moyron-Quiroz J, McCausland MM, Davies DH, Johnston RJ, Peters B, Rafii-El-Idrissi Benhnia M, Hoffmann J, Su H-P, Singh K, Garboczi DN, Head S, Grey H, Felgner PL, and Crotty S. 2008. Selective CD4+ T Cell Help for Antibody Responses to a Large Viral Pathogen: Deterministic Linkage of Specificities. Immunity 28: 847–858. [PubMed: 18549802]

40. Kang I, Barthold SW, Persing DH, and Bockenstedt LK. 1997. T-helper-cell cytokines in the early evolution of murine Lyme arthritis. Infection and Immunity 65: 3107–3111. [PubMed: 9234761]
41. Bockenstedt LK, Kang I, Chang C, Persing D, Hayday A, and Barthold SW. 2001. CD4+ T Helper 1 Cells Facilitate Regression of Murine Lyme Carditis. Infection and Immunity 69: 5264–5269. [PubMed: 11500394]
42. Gross DM, Steere AC, and Huber BT. 1998. T helper 1 response is dominant and localized to the synovial fluid in patients with Lyme arthritis. Journal of immunology (Baltimore, Md. : 1950) 160.
43. Sojka DK, Bruniquel D, Schwartz RH, and Singh NJ. 2004. IL-2 Secretion by $CD4^+$ T Cells In Vivo Is Rapid, Transient, and Influenced by TCR-Specific Competition. The Journal of Immunology 172: 6136–6143. [PubMed: 15128800]
44. Zhao C, and Davies JD. 2010. A peripheral CD4+ T cell precursor for naive, memory, and regulatory T cells. Journal of Experimental Medicine 207: 2883–2894. [PubMed: 21149551]
45. Nepom GT 2012. MHC class II tetramers. Journal of immunology (Baltimore, Md. : 1950) 188: 2477–2482. [PubMed: 22389204]
46. Bacher P, and Scheffold A. 2013. Flow-cytometric analysis of rare antigen-specific T cells. Cytometry Part A 83A: 692–701.
47. Wooldridge L, Lissina A, Cole DK, Van Den Berg HA, Price DA, and Sewell AK. 2009. Tricks with tetramers: how to get the most from multimeric peptide–MHC. Immunology 126: 147–164. [PubMed: 19125886]
48. Moon JJ, Chu HH, Pepper M, McSorley SJ, Jameson SC, Kedl Ross M., and Jenkins MK. 2007. Naive CD4+ T Cell Frequency Varies for Different Epitopes and Predicts Repertoire Diversity and Response Magnitude. Immunity 27: 203–213. [PubMed: 17707129]
49. Goldrath AW, and Bevan MJ. 1999. Selecting and maintaining a diverse T-cell repertoire. Nature 402: 255–262. [PubMed: 10580495]
50. Lythe G, and Molina-París C. 2018. Some deterministic and stochastic mathematical models of naïve T-cell homeostasis. Immunological reviews 285: 206–217. [PubMed: 30129198]
51. Bai X, Chi X, Qiao Q, Xie S, Wan S, Ni L, Wang P, Jin W, and Dong C. 2020. T Follicular Helper Cells Regulate Humoral Response for Host Protection against Intestinal Citrobacter rodentium Infection. The Journal of Immunology 204: 2754–2761. [PubMed: 32269096]
52. Koutsakos M, Lee WS, Wheatley AK, Kent SJ, and Juno JA. 2022. T follicular helper cells in the humoral immune response to SARS-CoV-2 infection and vaccination. Journal of Leukocyte Biology 111: 355–365. [PubMed: 34730247]
53. Wahl I, and Wardemann H. 2022. How to induce protective humoral immunity against Plasmodium falciparum circumsporozoite protein. Journal of Experimental Medicine 219: e20201313. [PubMed: 35006242]
54. Hastey CJ, Ochoa J, Olsen KJ, Barthold SW, and Baumgarth N. 2014. MyD88- and TRIF-independent induction of type I interferon drives naive B cell accumulation but not loss of lymph node architecture in Lyme disease. Infect Immun 82: 1548–1558. [PubMed: 24452685]
55. Baumgarth N 2021. The Shaping of a B Cell Pool Maximally Responsive to Infections. Annu Rev Immunol 39: 103–129. [PubMed: 33472004]
56. Liu N, Montgomery RR, Barthold SW, and Bockenstedt LK. 2004. Myeloid differentiation antigen 88 deficiency impairs pathogen clearance but does not alter inflammation in Borrelia burgdorferi-infected mice. Infect Immun 72: 3195–3203. [PubMed: 15155621]
57. McCarron MJ, Park PW, and Fooksman DR. 2017. CD138 mediates selection of mature plasma cells by regulating their survival. Blood 129: 2749–2759. [PubMed: 28381397]
58. Weisel FJ, Zuccarino-Catania GV, Chikina M, and Shlomchik MJ. 2016. A Temporal Switch in the Germinal Center Determines Differential Output of Memory B and Plasma Cells. Immunity 44: 116–130. [PubMed: 26795247]
59. Barbour AG, Jasinskas A, Kayala MA, Davies DH, Steere AC, Baldi P, and Felgner PL. 2008. A genome-wide proteome array reveals a limited set of immunogens in natural infections of humans and white-footed mice with Borrelia burgdorferi. Infect Immun 76: 3374–3389. [PubMed: 18474646]
60. Drecktrah D, and Samuels DS. 2018. Genetic Manipulation of Borrelia Spp. Curr Top Microbiol Immunol 415: 113–140. [PubMed: 28918538]

61. Angel TE, Luft BJ, Yang X, Nicora CD, Camp DG II, Jacobs JM, and Smith RD. 2010. Proteome Analysis of Borrelia burgdorferi Response to Environmental Change. PLOS ONE 5: e13800. [PubMed: 21072190]

62. Liang Fang T, Nelson FK, and Fikrig E. 2002. DNA Microarray Assessment of Putative Borrelia burgdorferi Lipoprotein Genes. Infection and Immunity 70: 3300–3303. [PubMed: 12011030]

63. Barthold SW, Hodzic E, Tunev S, and Feng S. 2006. Antibody-mediated disease remission in the mouse model of lyme borreliosis. Infect Immun 74: 4817–4825. [PubMed: 16861670]

Key Points

- *Bb* $Arp_{(152–166)}$ containing MHCII tetramers identify Arp-specific CD4 T cells
- Labeled tetramerized Arp identifies small numbers Arp-B cells after Bb infection
- Data indicate failure to maintain but not to induce Arp-response after infection

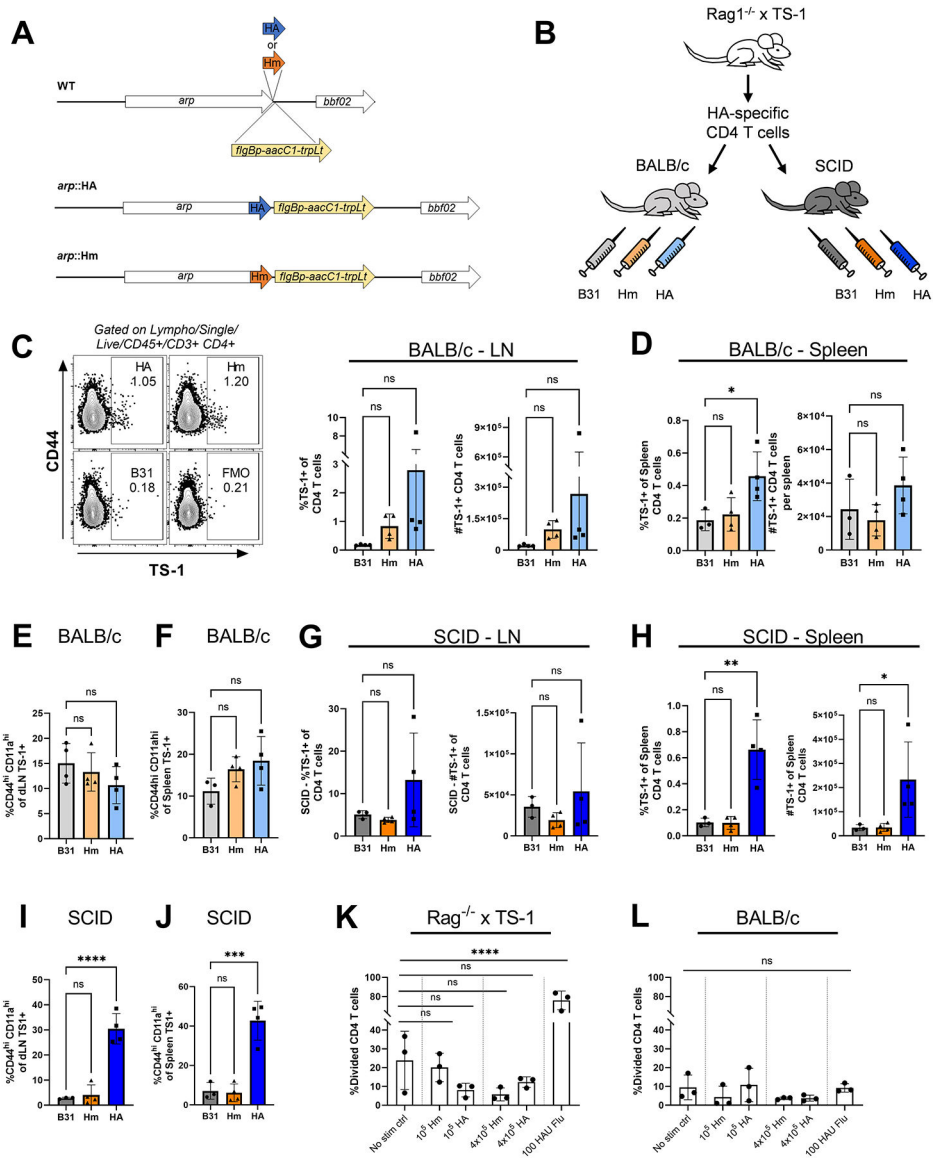

Figure 1. Mutant B. burgdorferi expressing $HA_{111–119}$ is infectious but does not stimulate HA-specific CD4 T cells.

(**A)** Schematic representation of constructs for generation of influenza hemagglutinin (HA) or E115K peptide (Hm) expressing mutant *Bb* B31. (**B)** Experimental design of HA-specific TS-1 CD4 T cell transfer to either BALB/c or BALB/c SCID recipients, followed by syringe inoculation with $HA_{111–119}$ expressing Bb, E115K expressing Bb, or parental B31 Bb strains. (**C)** Representative flow plots of TS-1+ CD4 T cells in the LN and (**D)** spleen of BALB/c recipients, 13 days post infection (dpi) with indicated Bb strains. Fluorescence minus one (FMO) sample was not stained with the anti-TS-1 TCR antibody. Summary data shown at right. (**E-F)** FACS analysis of percent of activated ($CD44^{hi}$ $CD11a^{hi}$) TS-1 cells in (**E)** dLN and (**F)** spleen of BALB/c recipients. (**G**) Quantitation of TS-1+ CD4 T cells in the dLN and **(H)** spleen of BALB/c SCID recipients 13 dpi as assessed by flow cytometry. (**I, J**) FACS analysis of percent of activated ($CD44^{hi}$ $CD11a^{hi}$) TS-1 cells in (**I)** dLN and (**J)** spleen of SCID mice. (**K, L**) Frequencies of divided (**K**) TS-1 CD4 T cells or (**L**) total

BALB/c CD4 T cells, cultured for 72h with irradiated splenic feeder cells and indicated stimuli. Cell proliferation was assessed by dilution of CFSE. Each symbol represents the result of one culture well, bars indicate mean, and error bars, SD. Data are representative of two independent experiments that produced similar results. *$p < 0.05$; **$p < 0.01$; ***$p < 0.001$; ****$p < 0.0001$. n.s. not significant by Student's *t*-test.

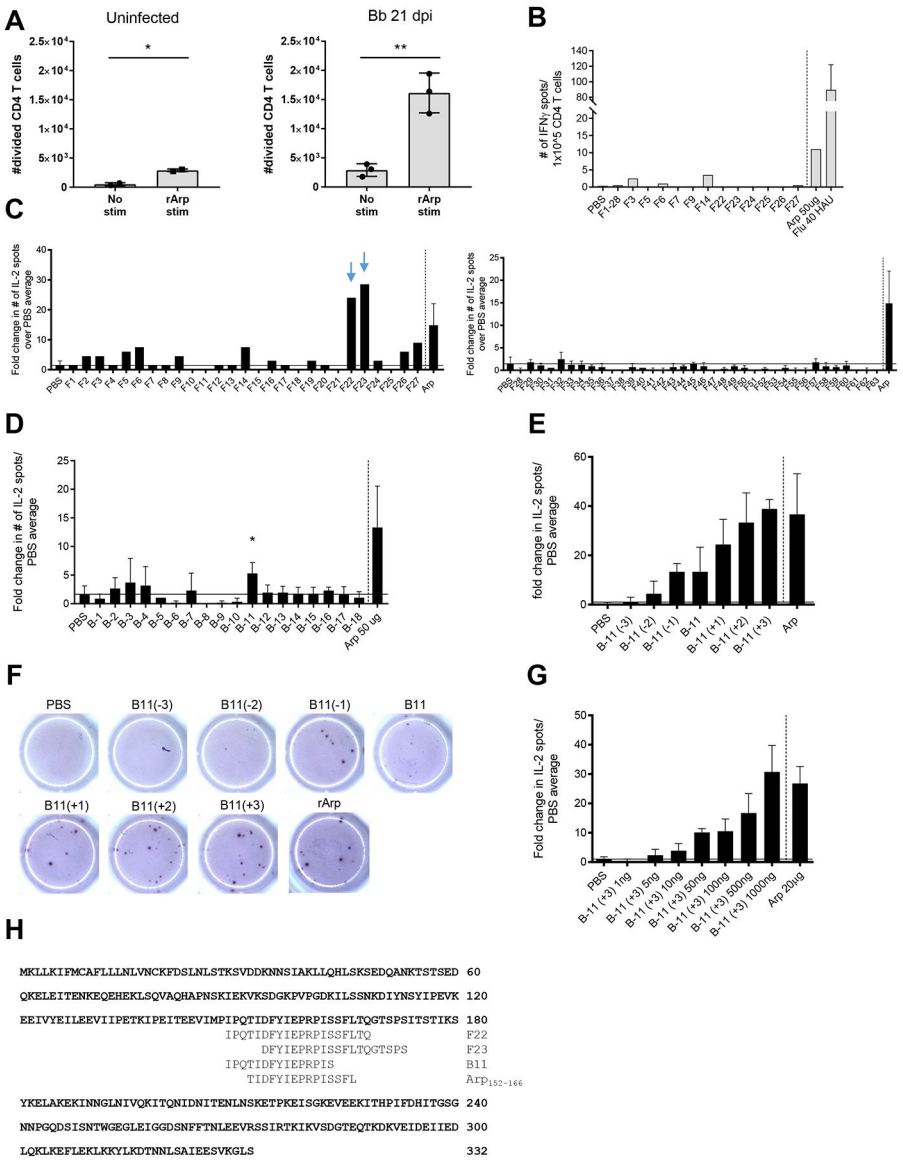

Figure 2. Discovery of an immunodominant Arp epitope.

(A) Mean ± SD of frequencies divided CFSE-labeled CD4 T cells from 3 replicates of LN cells from Bb infected mice 21 dpi, or uninfected controls cultured for 6 days with/without rArp. *p < 0.05, **p < 0.01 by Student's *t*-test. (**B, C)** CD4 T cells from Bb infected mice (12 dpi) were stimulated with irradiated splenic feeder cells plus Arp gene-wide overlapping 20-mer Arp peptides (100 μg per well), recombinant Arp (50 μg per well), or PBS, and analyzed for (**B**) IFNγ or (**C**) IL-2 secretion by ELISPOT. (**B**) Shown are mean numbers of IFNγ ELISPOTS, n=3/stimulus. CD4 T cells from influenza A/PR8 infected mice (7 dpi) were stimulated with 40 HAU of inactivated virus as a positive control. (**C**) Shown are mean fold-changes in IL-2 ELISPOT compared to average of PBS induced IL-2 ELISPOT; arrows indicate Arp peptides with consistently strong induction of IL-2 production. **(D)** Immunogenic regions identified in (C) were further probed through stimulation with 15-mer Arp peptides B1–B18 and (**E, F**) 15-mer Arp peptides offset

by 1 aa residue. Controls were recombinant Arp and PBS. Mean fold-induction of IL2 ELISPOTS over PBS control. Asterisk indicates significant induction above the mean of the background. **(F)** Representative images of ELISPOT wells. (**G)** Mean fold-change in IL-2 ELISPOTS compared to mean of PBS controls in response to graded doses of peptide B11(+3) peptide. (**H)** Alignment of selected Arp peptide sequences and $Arp_{152–166}$ epitope to the Arp protein sequence. **B-E**, **G,** data are representative of two (**B, D, E, G**) or three (**C**) independent experiments.

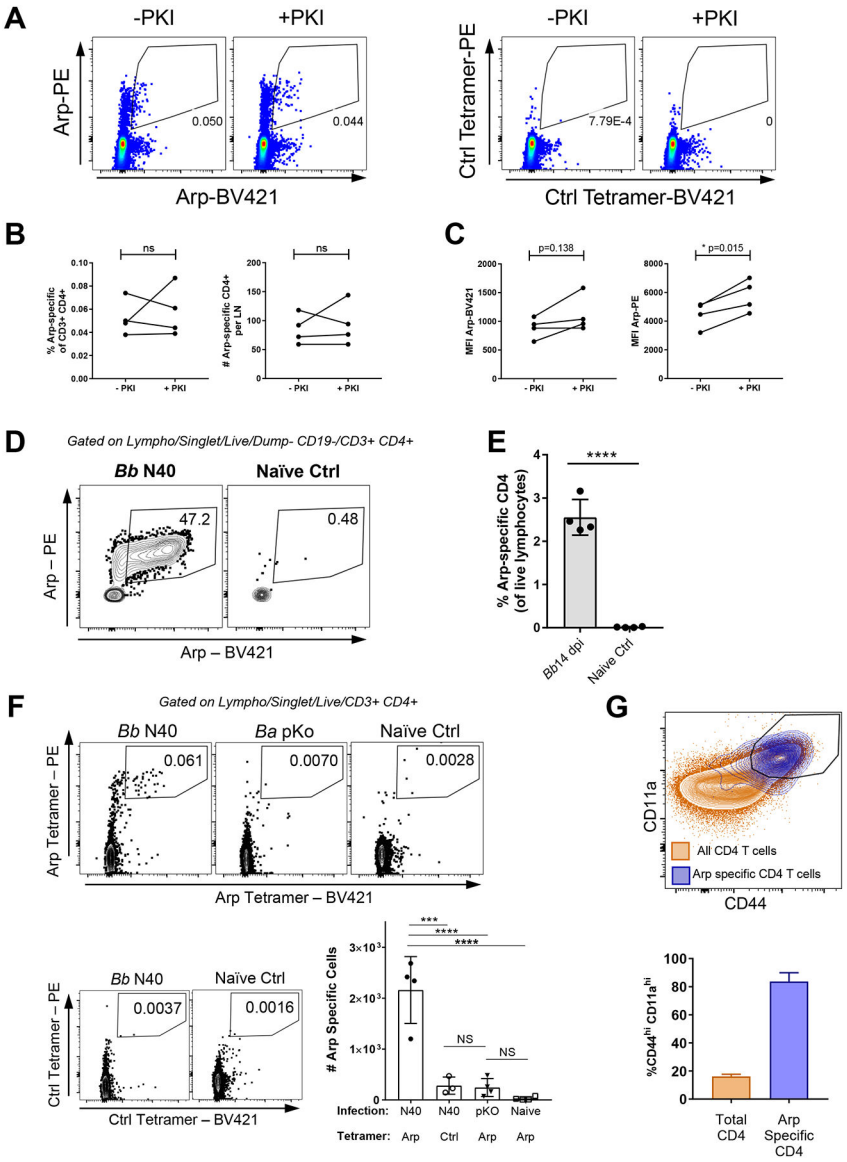

Figure 3. Arp tetramer detects Bb Ag-specific CD4 T cells.

(**A**) Representative flow cytometry plots of draining LN from 14 dpi *Bb* infected mice. LN cells from individual mice were either treated with a protein kinase inhibitor (+PKI) or incubated in staining media (-PKI) prior to incubation with Arp tetramer. Plots are pre-gated on live single lymphocytes, CD19- CD3+ CD4+. (**B**) Frequencies and numbers of Arp-specific CD4 T cells detected in draining LN of 14 dpi Bb infected mice. (**C**) Mean fluorescence intensity (MFI) of BV421- and PE-labeled Arp tetramer among CD4+ T cells. (**D**) Representative flow cytometry plots showing LN cells from 14 dpi *Bb* N40 infected and naïve control mice following enrichment by magnetic pull down of tetramer-labeled cells. (**E**) Frequency of Arp-specific CD4 T cells among enriched fractions of lymphocytes from 14 dpi *Bb* infected (n=4) and naïve (n=4) mice. Data are representative of three independent experiments. **F**) Flow cytometry plots showing dual Arp-tetramer-labeling of CD4 T cells from the draining LN 14 dpi *Bb* N40-infected, *B. afzelii* PKo-infected, or naïve control

mice (n=4 mice for each condition). Staining with non-specific control tetramer stains for Bb N40 and naïve mice is shown below. Bottom right bar chart shows summary of results. (**G**) Overlay 5% contour plot with outliers of staining for CD44 and CD11a among total and Arp-specific CD3+ CD4+ T cells in the draining LN of 14 dpi Bb N40 infected mice (n=4). Bar chart shows mean frequencies ± SD of activated $CD44^{hi}$ $CD11a^{hi}$ cells. **B, C,** n=4 mice, paired two-tailed Student's *t*-test, *p < 0.05. **E**) Two-tailed Student's *t*-test; **F**) One-way ANOVA with Tukey's post-hoc comparison. ***p < 0.001, ****p < 0.0001. Results in A-E are representative of two experiments that gave comparable results. F, Results are from one side-by-side comparison analysis of all three Bb strains. G, analysis is one of at least 4 experiments showing similar results.

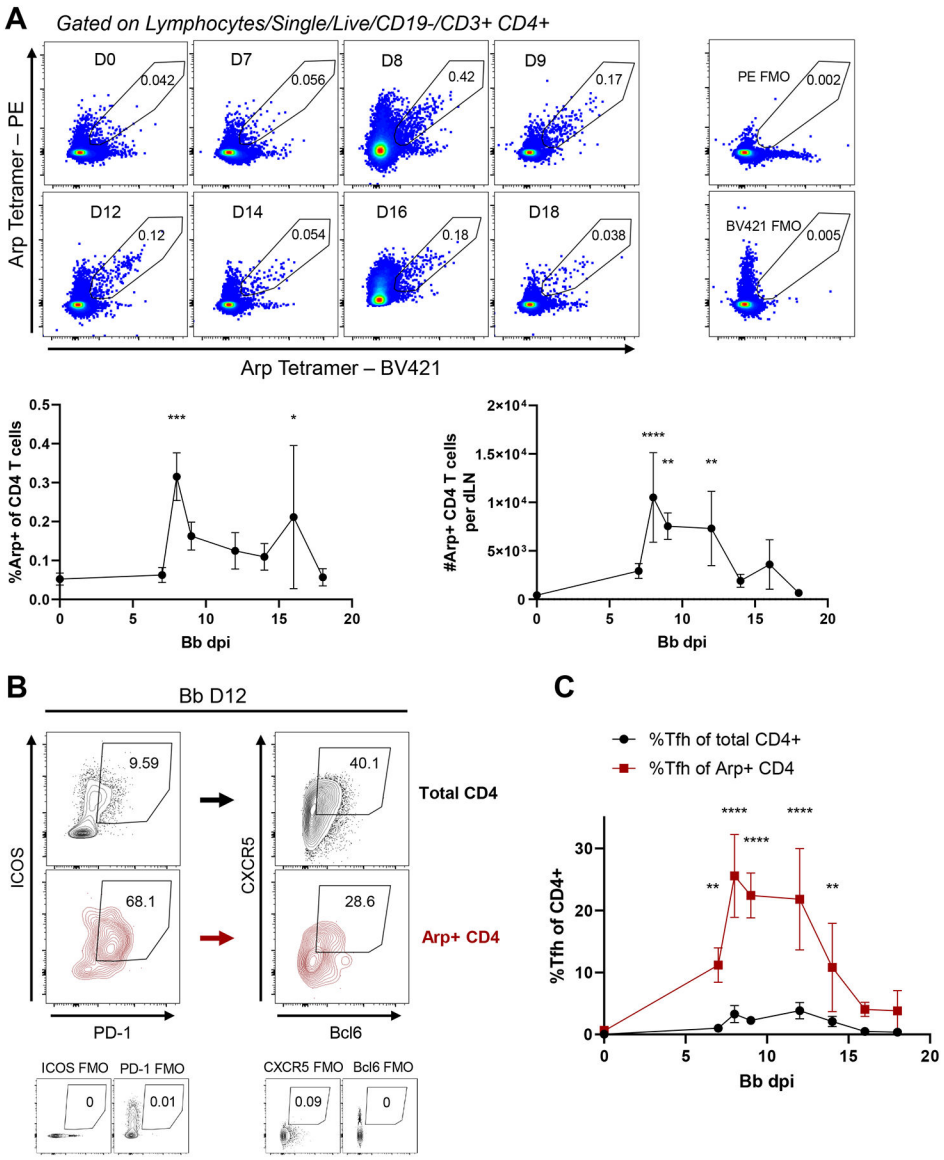

Figure 4. $Arp_{152–166}$ specific CD4 Tfh cells contract early after Bb infection.

(A) Representative flow cytometry plots of Arp tetramer-binding CD4 T cells from the dLN of mice infected with host-adapted Bb N40 at indicated dpi. “Fluorescence minus one” (FMO) tetramer controls at right. Bottom, summary of results (frequencies, left and cell counts, right). (**B**) Representative contour flow cytometry plots of total (top) and Arp-specific (bottom) CD4+ ICOS+ PD-1+ CXCR5+ Bcl6+ Tfh. (**C**) Summary data of percent Tfh, gated as shown in (**B**). Multiple paired t-tests, FDR=2%. N = 4 mice, each timepoint. **(A)** One-way ANOVA with Dunnet’s multiple comparisons test; significant difference compared to 0 dpi as indicated. (**B**). Multiple paired t-tests, FDR=2%. N=4 mice, each timepoint as indicated. *p < 0.05, **p < 0.01, ***p < 0.001, ****p < 0.0001. Results are from one complete time course experiment. Individual time points have been repeated 0 – 4 times.

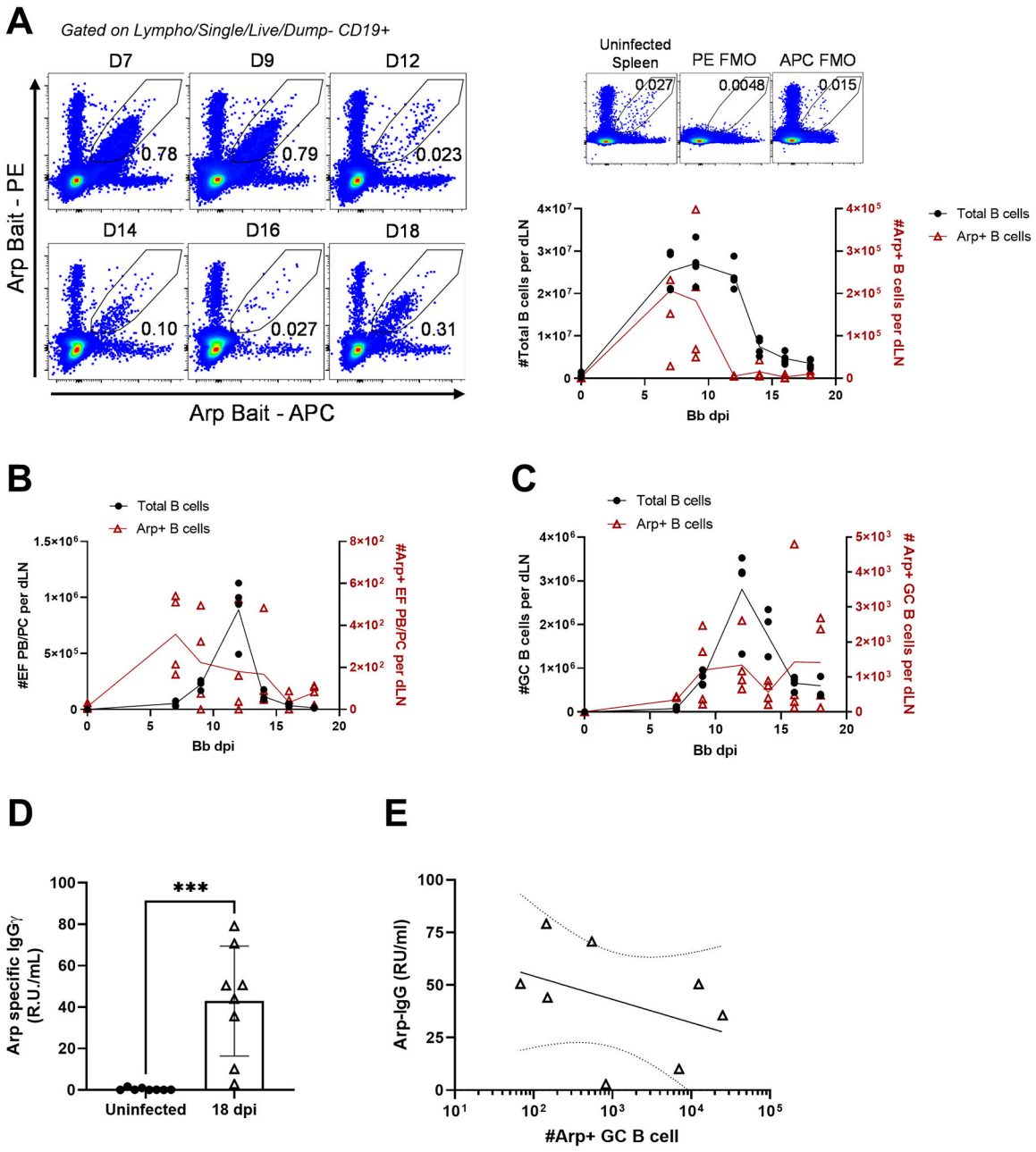

Figure 5. Tetrameric Arp bait identifies small numbers Arp-specific B cells.

(**A)** Representative flow cytometry plots of dLN of Bb-infected C57BL/6 mice at indicated dpi. Top right: uninfected control and "fluorescence minus one" (FMO) B cell bait controls. Bottom right: Individual cell counts of total CD19+ B cells (left y-axis, black) and Arp-specific B cells (right y-axis, red), lines indicate mean/group. (**B**) Cell counts of total (black, left y-axis) and Arp-specific (red, right y-axis) extrafollicular (EF) plasmablasts (PB) and plasma cells (PC), defined as CD19+ CD45R^{lo} CD138+ TACI+. (**C**) Cell counts of total (black, left y-axis) and Arp-specific (red, right y-axis) GC B cells, defined as CD19+ CD45R^{hi} CD24^{hi} CD95+. Results are from n =4 mice per time point of one complete time course experiment performed. Additional analysis of individual timepoints done 0 – 2 times

(**D)** Relative unit Arp-IgG in sera from mice before and at 18 dpi with Bb N40, assessed by ELISA. Each dot represents results from one mouse (n = 8/group) bar indicates mean, line SD. (**E)** Semi-log non-linear regression plot of total Arp+ GC B cells compared to serum Arp-IgG. Dotted line shows 95% CI. (**D-E**, data are pooled from two independent experiments, n=8 total. (D) ***$p < 0.001$ by two-tailed Student's *t*-test.

Table 1.

Oligonucleotides

Name	Sequence
arp_155F	CCAATAAAACTTCTACCTCA
arp_996R+HA+AaAg	*__ACCGGT__TAA__GACGTC__TTA *TTTAGGAAAAATTTCAAATCTTTCAAA*ACTTAAACCCTTTACACTT
arp_996R+Hm+AaAg	__ACCGGT__TAA__GACGTC__TTA *TTTAGGAAAAATTT__T__AAATCTTTCAAA*ACTTAAACCCTTTACACTT
arp_978F+AatII	__GACGTC__AAGTGTAAAGGGTTTAAGTT
arp_D1773R+AgeI	__ACCGGT__GGAATCCAATAACAAAGTTC
arp_780F	TGATAGCAATTTCTTTACCA
arp-663F	TACACACCCCATATTTGATCACATTACT
arp-767R	TTGCTATCACCACCAATTTCAAGT
arp-705P	TCCCGGACAAGATTCTATATCCAATACATGGG
flab-571F	GCAGCTAATGTTGCAAATCTTTTC
flab-677R	GCAGGTGCTGGCTGTTGA
flab-611P	AAACTGCTCAGGCTGCACCGGTTC

* Nucleotides in **bold** are engineered restriction sites and nucleotides in *italics* are the $HA_{111–119}$ or E117K mutant $HA_{111–119}$ sequences.

Table 2.

Arp sequence homology

Species	Strain	Geography	Source	OspC Type	Peptide Length	% Amino Acid Identity to N40	*arp* gene location	NCBI protein accession #
B. burgdorferi	N40	New York	*Ixodes scapularis*	E	332 aa	100	lp28–5	WP_010890266.1
B. burgdorferi	64b	New York	Human	B1	332 aa	100	lp28–5	WP_010890266.1
B. burgdorferi	118a	New York	Human	J	332 aa	100	lp28–5	WP_010890266.1
B. burgdorferi	156a	New York	Human	H2	332 aa	100	lp28–5	WP_010890266.1
B. burgdorferi	B31	New York	*Ixodes scapularis*	A	332 aa	100	lp28–1	WP_010890266.1
B. burgdorferi	PAbe	Germany	Human	--	332 aa	100	lp28–1	WP_010890266.1
B. burgdorferi	JD1	Massachusetts	*Ixodes scapularis*	C1	332 aa	99.1	lp28–4	WP_014540454.1
B. burgdorferi	72a	New York	Human	G	332 aa	92.15	lp36	WP_012665889.1
B. burgdorferi	94a	New York	Human	U1	332 aa	91.84	lp36	WP_012672552.1
B. afzelii	PKo	Germany	Human	--	--	--	--	--
B. garinii	PBr	Denmark	Human	--	--	--	--	--